Nuclear Instruments and Methods in Physics Research B 307 (2013) 177–180

Contents lists available at SciVerse ScienceDirect

Nuclear Instruments and Methods in Physics Research B

journal homepage: www.elsevier.com/locate/nimb

Fabricating vertically aligned ultrathin graphene nanosheets without any catalyst using rf sputtering deposition

Jian-Hua Deng [a], Shao-Long Wu [b], Yu-Mei Yang [b], Rui-Ting Zheng [b], Guo-An Cheng [b,*]

[a] College of Physics and Electronic Information Science, Tianjin Normal University, Tianjin 300387, PR China
[b] Key Laboratory of Beam Technology and Material Modification of Ministry of Education, College of Nuclear Science and Technology, Beijing Normal University, Beijing 100875, PR China

ARTICLE INFO

Article history:
Received 30 September 2012
Received in revised form 28 November 2012
Accepted 2 December 2012
Available online 18 January 2013

Keywords:
Graphene nanosheet
Radio frequency sputtering
Field emission

ABSTRACT

Ultrathin graphene nanosheets (GNSs) were synthesized on Si substrates by using radio frequency sputtering deposition. SEM, TEM and Raman were employed to characterize the GNSs. The GNSs are well aligned on the Si substrates with sharp edges separated and unfolded outside. The TEM observation shows that most of the GNSs are less than 10 layers. The field emission properties of the GNSs synthesized for 10 h were also studied. They show good field emission characteristics, with a low turn-on electric field of 2.522 V/μm, a large field enhancement factor, and excellent stability behavior, suggesting promising prospects in the application of field electron emitting devices.

© 2013 Elsevier B.V. All rights reserved.

1. Introduction

Graphene research has developed at a relentless pace since its discovery in 2004 [1]. Numerous applications based on graphene have been tried due to its incomparable physical properties [2,3]. However, the synthesis of mono-layer graphene is usually low yield and the products are hard to be purified, it is thus very important to synthesize some other material behaves like graphene but is easy to be fabricated. Based on this purpose, few-layer graphene nanosheets (GNSs) were synthesized. The fabrication of ultrathin GNSs has been reported by Wang and his coworkers in 2004 [4,5]. They presented an inductively coupled radio-frequency plasma enhanced chemical vapor deposition (rf–PECVD) method to prepare single-, bi-, and few-layer GNSs, and they also proposed a possible 2-dimensional GNS growth mechanism [6]. However, the traditional CVD growth of graphene usually involves high temperature decomposition of carbonaceous gas and catalysts, which results in the growth of graphene with a high rate and makes the growth process less controllable [7–10].

In this study, we developed a controllable way to fabricate few-layer GNSs without any catalyst on Si substrates by using rf sputtering deposition, and the field emission (FE) characteristics of the well aligned ultrathin GNSs were studied.

2. Experimental details

The growth of GNSs was carried out by using a capacitively coupled rf (13.56 MHz) sputtering system schematically shown in Fig. 1. Hydrogen was not only used for glow discharge but also for sputtering carbon which comes from a high-purity graphite target. The vacuum chamber was pre-pumped to 8.0×10^{-4} Pa, and the Si substrate was then heated to 700 °C in hydrogen ambient at 300 Pa. The distance between the graphite target and the Si substrate was about 6 cm. During the growth of GNSs, the rf power, the substrate temperature, the gas flow and the pressure were 300 W, 700 °C, 2.5 sccm and 300 Pa, respectively. The growth time was 1 h, 5 h and 10 h, respectively.

The FE testing system has been described previously in detail [11,12]. In short, a diode configuration with the prepared GNSs as the cathode against a stainless steel plate as the anode was employed, and the distance between the cathode and the anode was 1 mm. The base pressure and the cathode temperature during the FE measurements were $\sim 1 \times 10^{-7}$ Pa and ~288 K, respectively. The experimental data was automatically recorded by a computer in terms of emission current *versus* applied voltage (*I–V*).

Field emission scanning electron microscope (SEM, JSM-4800) was utilized to observe the morphology of the GNSs, and high resolution transmission electron microscope (HRTEM, TECNAI F30) was employed to characterize their fine structures. Structural information of the GNSs was also determined by Raman Spectroscopy (LavRAM Aramis) with a laser wavelength of 633 nm. The

* Corresponding author. Tel./fax: +86 10 62205403.
E-mail address: gacheng@bnu.edu.cn (G.-A. Cheng).

0168-583X/$ - see front matter © 2013 Elsevier B.V. All rights reserved.
http://dx.doi.org/10.1016/j.nimb.2012.12.120

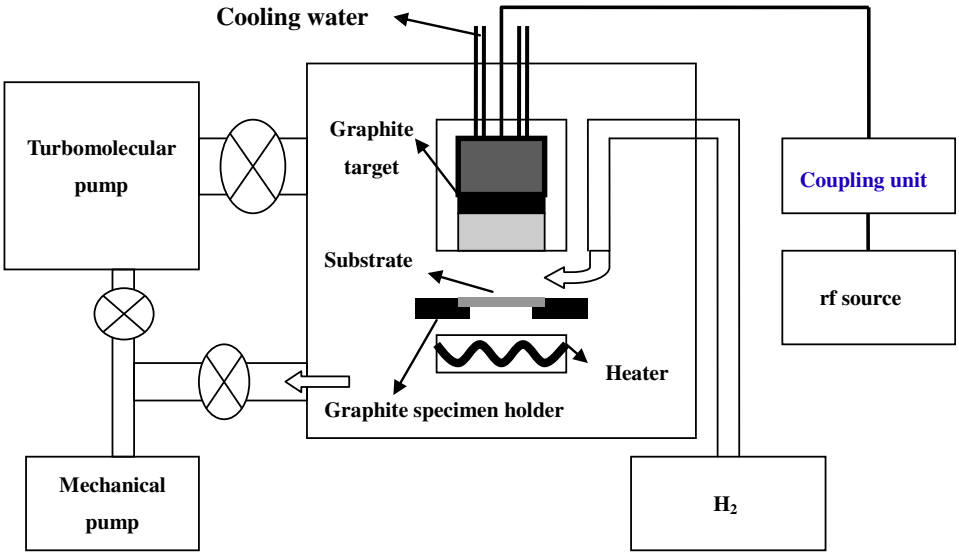

Fig. 1. Schematic illustration of the capacitively coupled rf sputtering system used for the GNS growth.

work function of the GNSs was measured by using photoelectron spectrometer (AC-2 RIKEM KEIKI).

3. Results and discussion

Morphological evolution of the GNSs with the growth time can help us understand their growth process. Fig. 2 shows SEM top-view images of the GNSs synthesized for 1 h (Fig. 2a), 5 h (Fig. 2b), and 10 h (Fig. 2c), respectively, and the insets are the corresponding SEM side-view images. In the first growth hour, there are spot-like and needle-like nano-structures appearing on the Si substrates, and this phase is believed to be related to the nucleation of the GNSs [11]. And then, the GNSs grow according to a quasi-2-dimensional growth model. The height of GNSs reaches about 400 nm after 10 h hydrogen plasma processing (inset of Fig. 2c). The GNSs are separated from each other with sharp edges unfolded outside, and this morphology is believed to be beneficial for FE due mainly to a less field screening effect [13].

Further structural information revealing the morphological evolution with the growth time was determined by Raman spectroscopy with a laser wave length of 633 nm, as shown in Fig. 3. For all types of GNSs, symmetric single 2D peak around 2662 cm^{-1} is observed, which stems from the second order of the zone-boundary phonons and is closely related to the layer number of graphene [14–16]. The height ratio of 2D peak and G peak, h_{2D}/h_G, has usually being adopted to evaluate graphenes. Larger h_{2D}/h_G ratio is in conformity with graphene of few layers [14]. The h_{2D}/h_G ratio of the GNSs synthesized for 10 h is ~1.16, demonstrating that these GNSs are ultrathin graphenes. While the h_{2D}/h_G ratios of the GNSs synthesized for 1 h and 5 h are comparatively smaller, due mainly to the defective carbon layer pre-deposited on the Si substrates also contributes to the Raman G peak, but in our calculation by using the h_{2D}/h_G ratio, only Raman contribution to G peak generated by graphenes can be taken into consideration, this extra Raman contribution to G peak from the defective carbon layer results in the decrease of the h_{2D}/h_G ratio and makes the evaluation inaccurate. However, we can conjecture that the percentage of this Raman contribution to G peak from the defective carbon layer decreases with the increasing coverage of GNSs on the Si substrates, it is thus reasonable to evaluate the GNSs by using h_{2D}/h_G ratio when the Si substrates are covered by GNSs, referring to GNSs synthesized for 10 h shown in Fig. 2c. The peak centered at 1332 cm^{-1} reveals that our GNSs are defective.

The morphological study indicates that the growth of GNSs undergoes two main phases: nucleation and 2-dimensional growth. Pre-depositing a defective carbon layer on the Si substrates to provide defective locations is indispensable during the nucleation of GNSs [11]. The 2-dimensional growth process, referring to a carbon atom diffusion process on the surface of graphene, has been discussed previously in detail [6,17–19].

The fine structure of the GNSs synthesized for 10 h was observed by HRTEM. Fig. 4a is a low-resolution TEM image of the GNSs, showing that the GNSs are aggregated; we consider that this may arise from the sonication of GNSs in alcohol during the preparation of TEM samples since nearly all nano-materials are inclined to aggregation to lower their surface energy. Fig. 4b is a HRTEM image of a curled-up GNS edge, showing that the GNS has about nine layers. In fact, during the TEM observation, the vast majority of GNSs are less than 10 layers, having parallelly stacked inner layers and defective outer shells.

Fig. 5a shows the FE characteristics of the vertically aligned ultrathin GNSs synthesized for 10 h presented in terms of emission current density *versus* applied fields, namely, the *J*–*E* curve. The turn-on electric field (E_{on}, applied field when *J* is 10 μA/cm^2) and the threshold field (E_{th}, applied field when *J* is 1 mA/cm^2) are 2.522 and 3.401 V/μm, respectively, and the largest *J* is about 4 mA/cm^2. The inset of Fig. 5a is the corresponding FN plots, the nearly linear relationship between $\ln(J/E^2)$ and $1/E$ reveals that the emitted electrons are extracted by the applied fields [20]. By applying the FN model [20], the field enhancement factor (β) is determined by the slope of FN curve (~38.96) and the work function of the GNSs (4.69 eV): 1781. β is a parameter strongly dependent on the electron tunneling at the emission sites, and this large β of the GNSs can facilitate the electron tunneling through barriers, namely, can improve the FE properties of the GNSs. It can be found that the FE properties of the GNSs are better than that of a great many low dimensional field emitters, such as carbon nano-fibers [21], carbon nano-tips [22], flat-lying single-layer grapheme [23], and even approach that of carbon nanotubes [24]. We attribute the eminent FE properties of the GNSs, on the one hand, to the separated, unfolded and sharp edges of the GNSs which are effective

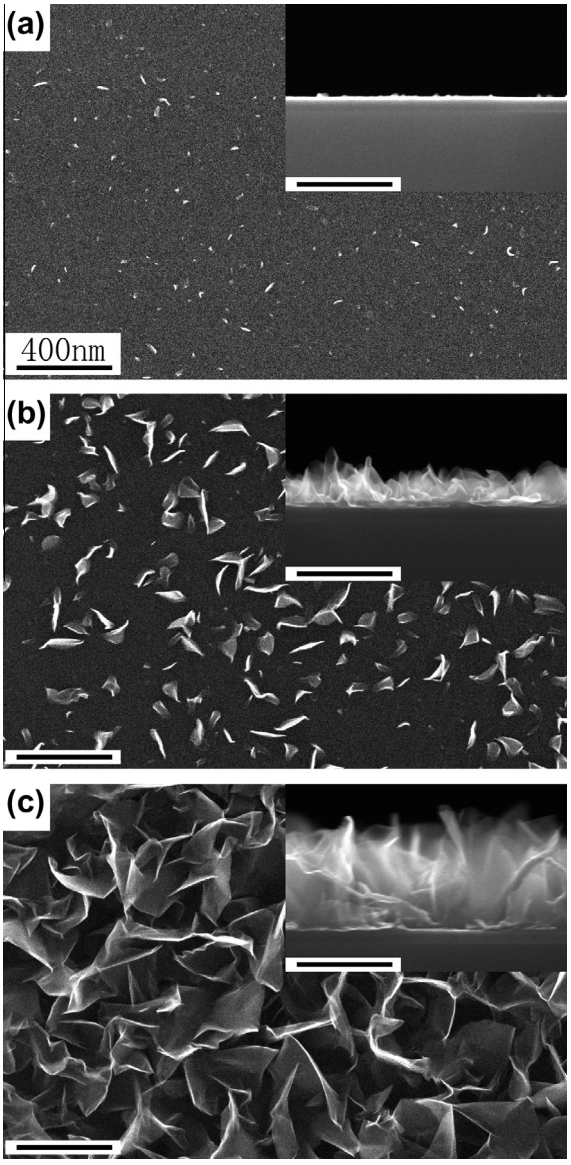

Fig. 2. SEM top-view images of GNSs synthesized for (a) 1 h, (b) 5 h, and (c) 10 h, respectively, and the insets are the corresponding SEM side-view images. Other growth conditions: 300 W, 300 Pa, H_2 (2.5 sccm), 700 °C. All the scale bars are 400 nm.

emission sites during FE, and on the other hand, to the vacancy-related defects generated from atomic collision during the hydrogen plasma processing that provide a great many effective emission sites [25].

Fig. 5b shows the stability behavior of the GNSs synthesized for 10 h (GNSs-10 h) at an applied field of 3.200 V/μm. We employ a parameter J_{drop} (J degradation during the testing time, calculated by $(J_{first} - J_{last})/J_m$, J_{first}, J_{last} and J_m are the first, the last and the mean emission current density, respectively) to evaluate the FE stability behavior of the emitters.

The J_{drop} of the GNSs-10 h is negligible (1.481%). We attribute this excellent FE stability to the unique 2-dimensional structure of the GNSs which ensures a relatively uniform current distribution on its surface and greatly prevents the effective emission sites from being burned off by Joule heat [26]. The above results have suggested a promising potential for using the GNSs as high-performance field emitters.

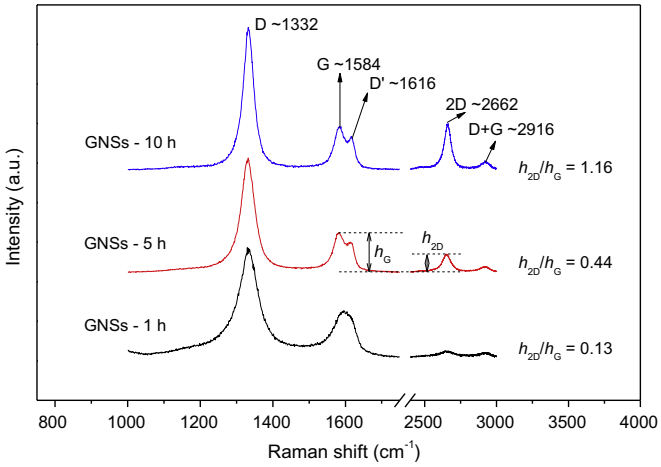

Fig. 3. Raman spectra (633 nm laser wavelength) of GNSs synthesized within different durations. h_{2D} and h_G are heights of Raman 2D peak and G peak, respectively.

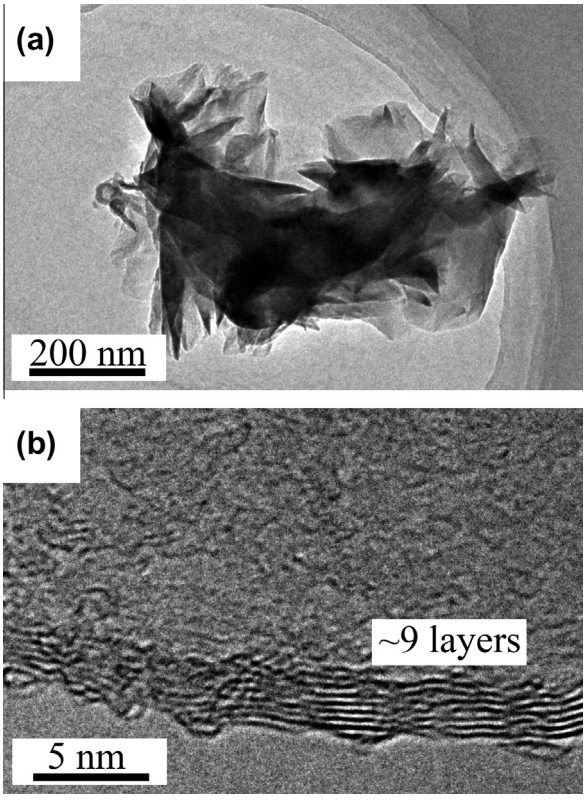

Fig. 4. TEM images of the GNSs synthesized for 10 h. (a) Low-resolution TEM image. (b) High-resolution TEM images of a curved GNS edge with about nine layers. Other growth conditions: 300 W, 300 Pa, H_2 (2.5 sccm), 700 °C.

4. Conclusions

Ultrathin GNSs have been synthesized in hydrogen ambient without any catalyst by using rf sputtering deposition at 700 °C on Si substrates. The morphological evolution with the growth time study indicates that the growth of GNSs undergoes two phases: nucleation and 2-dimensional growth. The HRTEM observation reveals that our GNSs synthesized for 10 h are less than 10 layers in most cases. The GNSs synthesized for 10 h show good FE properties.

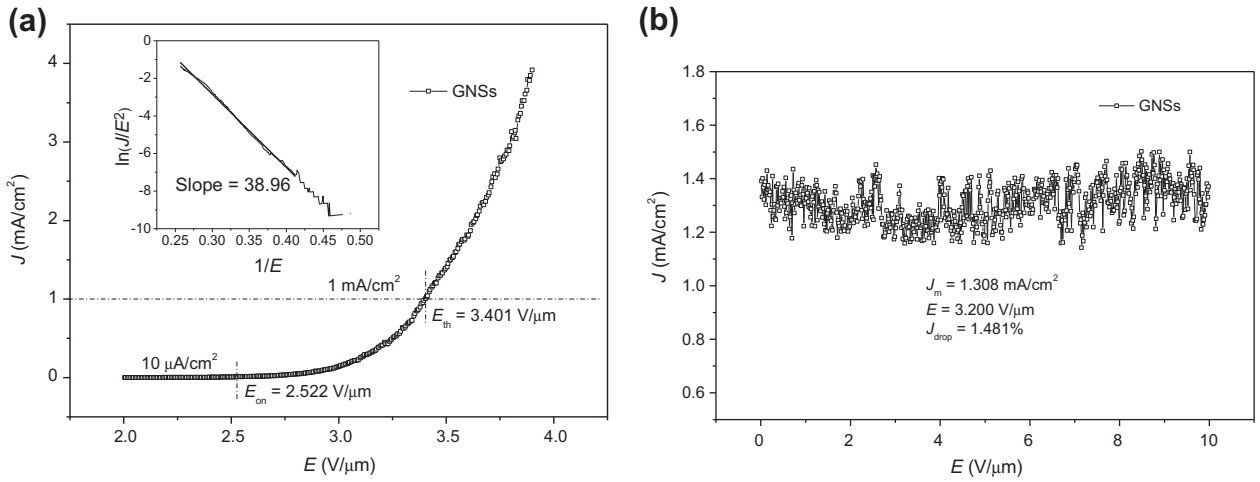

Fig. 5. FE properties of the GNSs synthesized for 10 h. (a) *J*–*E* curve, the inset is the corresponding FN plots. (b) 10 h stability behavior, J_m: mean emission current density, J_{drop}: *J* degradation during the testing time.

They have a low E_{on} of 2.522 V/μm and E_{th} of 3.401 V/μm, a large field enhancement factor of ~1781, and excellent stability (1.481% emission current degradation in 10 h), suggesting promising prospects in the application of high-performance field electron emitting devices.

Author contributions

J.H.D. conceived and carried out the experiment, characterized the samples, led the data analysis, proposed theoretical interpretation and wrote the manuscript; S.L.W. and Y.M.Y. assisted with the sample preparation; R.T.Z. and G.A.C. supervised the sample fabrication and characterization; G.A.C. edited the manuscript. All authors discussed the results and commented the manuscript.

Acknowledgments

This work is supported by the National Basic Research Program of China (No. 2010CB832905), Science and Technology Development Funds, Tianjin, P. R. China (No. 20120312), Application Development Funds of Tianjin Normal University, P. R. China (No. 52XK1207), the Natural Science Funds of Tianjin Normal University, P. R. China (No. 5RL119), the Open Research Fund of the Key Laboratory of Beam Technology and Material Modification of Ministry of Education, Beijing Normal University, P. R. China (No. 201208), and partially by the Key Scientific and Technological Project of the Ministry of Education of China (No. 108124).

References

[1] K.S. Novoselov, A.K. Geim, S.V. Morozov, D. Jiang, Y. Zhang, S.V. Dubonos, I.V. Grigorieva, A.A. Firsov, Electric field effect in atomically thin carbon films, Science 306 (2004) 666–669.
[2] A.K. Geim, K.S. Novoselov, The rise of graphene, Nat. Mater. 6 (2007) 183–191.
[3] M.J. Allen, V.C. Tung, R.B. Kaner, Honeycomb carbon: a review of graphene, Chem. Rev. 110 (2010) 132–145.
[4] J.J. Wang, M.Y. Zhu, R.A. Outlaw, X. Zhao, D.M. Manos, B.C. Holloway, V.P. Mammana, Free-standing subnanometer graphite sheets, Appl. Phys. Lett. 85 (2004) 1265–1267.
[5] J.J. Wang, M.Y. Zhu, R.A. Outlaw, X. Zhao, D.M. Manos, B.C. Holloway, Synthesis of carbon nanosheets by inductively coupled radio-frequency plasma enhanced chemical vapor deposition, Carbon 42 (2004) 2867–2872.
[6] M.Y. Zhu, J.J. Wang, B.C. Holloway, R.A. Outlaw, X. Zhao, K. Hou, V. Shutthanandan, D.M. Manos, A mechanism for carbon nanosheet formation, Carbon 45 (2007) 2229–2234.
[7] Y.H. Wu, B.J. Yang, Effects of localized electric field on the growth of carbon nanowalls, Nano Lett. 2 (2002) 355–359.
[8] S.K. Srivastava, A.K. Shukla, V.D. Vankar, V. Kumar, Growth, structure and field emission characteristics of petal like carbon nano-structured thin films, Thin Solid Films 492 (2005) 124–130.
[9] M.Y. Chen, C.M. Yeh, J.S. Syu, J. Hwang, C.S. Kou, Field emission from carbon nanosheets on pyramidal Si (100), Nanotechnology 18 (2007) 185706–185711.
[10] J. Kim, S.B. Seo, G.H. Gu, J.H. Suh, Fabrication of graphene flakes composed of multi-layer graphene sheets using a thermal plasma jet system, Nanotechnology 21 (2010) 095601–095611.
[11] J.H. Deng, R.T. Zheng, Y. Zhao, G.A. Cheng, Vapor-solid growth of few-layer graphene on carbon nanotubes using radio frequency sputtering deposition and its application on field emission, ACS Nano 6 (2012) 3727–3733.
[12] J.H. Deng, G.A. Cheng, Y.M. Yang, R.T. Zheng, Y. Zhao, Excellent field emission characteristics from few-layer graphene/carbon nanotube hybrids synthesized using radio frequency hydrogen plasma sputtering deposition, Carbon 50 (2012) 4732–4737.
[13] J.S. Suh, K.S. Jeong, J.S. Lee, I. Han, Study of the field-screening effect of highly ordered carbon nanotube arrays, Appl. Phys. Lett. 80 (2002) 2392–2394.
[14] A.C. Ferrari, J.C. Meyer, V. Scardaci, C. Casiraghi, M. Lazzeri, F. Mauri, S. Piscanec, D. Jiang, K.S. Novoselov, S. Roth, A.K. Geim, Raman spectrum of graphene and graphene layers, Phys. Rev. Lett. 97 (2006) 187401–187411.
[15] F. Tuinstra, J.L. Koenig, Raman spectrum of graphite, J. Chem. Phys. 53 (1970) 1126–1130.
[16] R.J. Nemanich, S.A. Solin, First- and second-order Raman scattering from finite-size crystals of graphite, Phys. Rev. B 20 (1979) 392–401.
[17] Y.H. Lee, S.G. Kim, D. Tománek, Catalytic growth of single-wall carbon nanotubes: an Ab intio study, Phys. Rev. Lett. 78 (1997) 2393–2396.
[18] O.A. Louchev, Y. Sato, H. Kanda, Growth mechanism of carbon nanotube forests by chemical vapor deposition, Appl. Phys. Lett. 80 (2002) 2752–2754.
[19] B. Lewis, J.C. Anderson, Nucleation and Growth of Thin Films, Academic Press Inc., London, 1979.
[20] R.H. Fowler, L.W. Nordheim, Electron emission in intense electric fields, Proc. R. Soc. London, Ser. A 119 (1928) 173–181.
[21] C.H. Weng, K.C. Leou, H.W. Wei, Z.Y. Juang, M.T. Wei, C.H. Tung, C.H. Tsai, Structural transformation and field emission enhancement of carbon nanofibers by energetic argon plasma post-treatment, Appl. Phys. Lett. 85 (2004) 4732–4734.
[22] C.L. Tsai, C.F. Chen, L.K. Wu, Bias effect on the growth of carbon nanotips using microwave plasma chemical vapor deposition, Appl. Phys. Lett. 81 (2002) 721–723.
[23] Z.S. Wu, S.F. Pei, W.C. Ren, D.M. Tang, L.B. Gao, B.L. Liu, F. Li, C. Liu, H.M. Cheng, Field emission of single-layer grapheme films prepared by electrophoretic deposition, Adv. Mater. 21 (2009) 1756–1760.
[24] J.-M. Bonard, H. Kind, T. Stöckli, L.-O. Nilsson, Field emission from carbon nanotubes: the first five years, Solid-State Electron. 45 (2001) 893–904.
[25] G. Wei, Emission property of carbon nanotube with defects, Appl. Phys. Lett. 89 (2006) 143111–143121.
[26] K.A. Dean, T.P. Burgin, B.R. Chalamala, Evaporation of carbon nanotubes during electron field emission, Appl. Phys. Lett. 79 (2001) 1873–1875.